Journal of Solid State Chemistry **151,** 298–307 (2000)
doi:10.1006/jssc.2000.8657, available online at http://www.idealibrary.com on IDEAL®

General Properties of Polycrystalline $LnNiO_3$ (Ln = Pr, Nd, Sm) Compounds Prepared through Different Precursors

M. T. Escote,* A. M. L. da Silva,† J. R. Matos,† and R. F. Jardim*

*Instituto de Física, Universidade de São Paulo CP 66318, 05315-970, São Paulo, SP, Brazil; and
†Instituto de Química, Universidade de São Paulo CP 26077, 05599-970, São Paulo, SP, Brazil

Received November 17, 1999; in revised form February 15, 2000; accepted February 18, 2000

We report on the synthesis and general physical properties of polycrystalline samples of $LnNiO_3$ (Ln = Pr, Nd, Sm). These compounds crystallize in a $GdFeO_3$-type orthorhombically distorted perovskite structure, *Pbnm* space group symmetry, and reveal a first-order metal–insulator transition in a large range of temperatures varying from ~130 to 400 K. The samples were prepared through three different methods: (1) the conventional ceramic process by mixing and reacting simple oxides; (2) through precipitation of hydroxides of Ln^{3+} and Ni^{3+} and (3) through sol–gel precursors. The samples were subjected to heat treatments at temperatures up to 1000°C and under oxygen pressures as high as 70 bar. Observations of the microstructure and measurements of X-ray powder diffraction XRD, electrical resistivity $\rho(T)$, and differential scanning calorimetric DSC, indicated important effects that precursors from different methods have upon the final properties of these compounds. A comparison between these characterizations revealed that sol–gel precursors resulted in better quality samples of $LnNiO_3$ compounds. © 2000 Academic Press

1. INTRODUCTION

Since the discovery of the first-order metal–insulator (MI) transition in orthorhombically distorted perovskite oxides of the general formula $LnNiO_3$ (Ln = rare earth), a great number of studies have been performed in order to better understand their general physical properties (1–4). Measurements of electrical resistance versus temperature on these compounds reveal the occurrence of a MI transition in a rather large range of temperature $130 \leq T_{MI} \leq 420$ K (2, 3). In fact, the metal–insulator transition temperature T_{MI} associated with such a transition was found to rise systematically as the size of the rare-earth ion decreases, being 130 K for $PrNiO_3$ and reaching values as high as 420 K in $EuNiO_3$ (5). These results also suggested that the MI transition is microscopically related with the degree of distortion of the ideal perovskite structure and, consequently, with the magnitude of the Ni–O–Ni bond angle (3). Neutron-diffraction experiments performed on either Pr or Nd compounds have also revealed that the MI transition is accompanied by a small structural change on their unit cell and that it takes place at T_{MI} (4). Furthermore, a combination of measurements involving transport and thermal analysis indicated that the character of the metal–insulator transition is of first order (6, 7). Additionally, to transport and thermal properties, these compounds have displayed interesting magnetic properties. For example, below T_{MI} both $PrNiO_3$ and $NdNiO_3$ compounds exhibit a magnetic ordering of the Ni sublattice though with an unusual magnetic structure (2).

Although all of the above properties are believed to be understood in these nickelates, the origin of the mechanism responsible for the appearance of the MI transition (structural, electronic, or magnetic) is still the object of some controversy (8–10). In fact, the discussion regarding this point requires extra experimental data and, consequently, available samples for these experiments. Taking into account these considerations, it is important to notice that the preparation of polycrystalline samples of these nickelates is rather difficult (1–9). This is because high-quality samples of these compounds requires sintering at both high temperatures and oxygen pressures (1–9).

The $LnNiO_3$ compounds (Ln = Y, La, Nd, Sm, Eu, Gd, Ho, Tm, Yb, Lu) were first produced by Demazeau *et al.* (1). Samples were prepared by mixing appropriate amounts of simple oxides (Ln_2O_3, NiO) and $KClO_3$. Few of these mixtures were enclosed in a sealed platinum crucible that was introduced into a belt-type pressure generator equipped with a microfurnace. Then, the mixture was heat-treated at 950°C and the decomposition of $KClO_3$ provided the necessary oxygen pressure (~60 bar) for the desirable phase formation. An alternative route for producing polycrystalline samples of these compounds was developed by Lacorre *et al.* (3) through sol–gel precursors by using as starting materials an intimate mixture of Ln_2O_3 and NiO dissolved in HNO_3. The mixture was subjected to heat treatment at temperatures higher than 1000°C and under oxygen

0022-4596/00 $35.00

pressures as high as 200 bar (1, 3). A combination of these processes was used by Vassiliou *et al.* (11), who prepared the $NdNiO_3$ compound through a mixture of simple oxides and sol–gel precursors. The mixture was submitted to heat treatments at 650°C under oxygen flux in order to reach single-phase $NdNiO_3$. More recently, Perez-Cacho and co-authors synthesized several of these nickelates through a citrate sol–gel route (12).

In this work, we focus on the preparation of polycrystalline samples of $LnNiO_3$ (Ln = Pr, Nd, Sm) through different routes. The interrelations between processing and properties of polycrystalline samples of $LnNiO_3$ were studied to gain information about the effects that precursors from different methods have upon the final properties of these compounds.

2. EXPERIMENTAL PROCEDURE

2.1. Sample Preparation

To simultaneously study the general physical properties of polycrystalline samples of $LnNiO_3$ (Ln = Pr, Nd, Sm) concerning the sample preparation techniques employed, samples were synthesized from three different methods: (1) mixture of simple oxides, (2) through synthesis of binary hydroxides, and (3) through sol–gel precursors, as described below.

2.1.1. Simple oxides. The first batch of samples was prepared from stoichiometric amounts of simple oxides, i.e., Pr_6O_{11} (Aesar 99.9%), Nd_2O_3 (Aesar 99.9%), Sm_2O_3 (Aesar 99.9%), and NiO (Aesar 99.9985%). To ensure stoichiometry, the first three oxides were heated at 900°C overnight to remove any absorbed water, and all weighting was performed in an atmosphere of ultra high-purity argon. For each sample, an amount of NiO was weighted first, and amounts of the other oxides were weighted to within 0.02% of the values calculated form the weight of NiO. All of the two oxides (Ln and Ni) were combined in a glass jar, tumbled to mix, and exposed to air for several hours so that the water vapor would be absorbed by the Ln oxides to prevent it from adhering to the glass.

The oxides were transferred directly to alumina crucibles and reacted at several sintering temperatures ranging from 700 to 1000°C for 72 h, with intermediate grinding. This resulted in black (Nd), brown (Pr), and gray (Sm) oxide mixtures, which were ground by hand with an agate mortar and pestle. The mixtures were not uniform, except the one containing Nd and Ni oxides. Unreacted Sm_2O_3 and Pr_6O_{11} were clearly visible in these mixtures. Samples prepared by this method, the so-called the conventional ceramic method, will be referred to as MO samples.

2.1.2. Hydroxide precipitation. The second batch was prepared through binary hydroxides of Ln^{3+} and Ni^{3+}. Few steps were necessary for producing these hydroxides, as follows. A stoichiometric aqueous suspension of the simple oxide Ln_2O_3 (Aesar 99.9%) and $NiCO_3$ (Aesar 99%) was dissolved in hydrochloric acid solution in a beaker. A solution of sodium hypochlorite was added to the latter solution to promote the Ni^{2+} to Ni^{3+} oxidation. After this step, a solution of sodium hydroxide was added slowly to the beaker until a pH $\sim$12 was reached. Under these conditions, the oxidation and simultaneous precipitation of the binary metallic hydroxide occurred. These powders were washed with deionized water several times until the filtrate gave a negative chloride ion test. They were collected, dried in vacuum, and transferred to an alumina crucible. The powders were subjected to heat treatments at 300 and 500°C in air for 40 h.

2.1.3. Sol–gel process. The third batch of polycrystalline samples of $LnNiO_3$ was prepared through sol–gel precursors (13). For this purpose, a solution was obtained from the adequate mixture of $Ln(NO_3)_3.6H_2O$ (Aesar 99.9%) and $Ni(NO_3)_2.6H_2O$ (Aesar 99.9985%), which were dissolved in $\sim$200 ml of water in a large beaker. A 50 mol% excess of solid citric acid monohydrate ($C_6H_8O_7.H_2O$) was added to the solution until it was completely dissolved under stirring and low heating, after which excess of ethylene glycol ($C_2H_6O_2$) was added to the solution. The solution was placed on a hot plate at $\sim$100°C and stirred magnetically, resulting in decomposition of the nitrates and the evolution of NO_2 gas. When the solution become colloidal, it was transferred to an alumina crucible and dried on the hot plate. Thereafter, the crucible was transferred to a muffle furnace and the temperature was raised to $\sim$300°C. At this temperature, the gel usually ignited (it was clearly visible), with the organic precursor partially decomposing into the simple oxides, as identified by X-ray diffraction analysis and evidenced by the formation of a dark brown powder. Complete oxidation of the organic material was achieved after heat treatment at 500°C for about 40 h.

2.2. Heat and Pressure Treatment

All the powders obtained by the three different methods were heat treated at temperatures ranging from 650 to 1000°C under oxygen pressures as high as 70 bar in a home-made furnace. The high-pressure and high-temperature sample space is provided by a thick-walled (14 mm) INCONEL 610 tube which is inserted in a tubular Lindberg furnace. This tube is closed by flanges with copper gasket seals and connected at one end to the gas-handling system by a swage-type fitting. The flange at the other end provides access to the sample space. The tube is refrigerated by water that flows in annular spaces surrounding the tube at both ends.

After these heat treatments, the samples were ball milled for 1 h with a centrifugal unit using an agate jar and balls to

obtain improved homogeneity. The resultant fine powder was pressed into pellets in a stainless-steel die at a pressure of $\sim$1 kbar. The pellets were returned to the alumina crucibles and sintered under oxygen pressure of $\sim$70 bar at 1000°C for 72 h, after which the furnace was cooled to room temperature in 12 h. The samples were dense and cohesive in nature, dark in color, and cylindrical in shape.

2.3. X-Ray Diffraction

Phases were identified by means of X-ray powder diffraction measurements using Cu$K\alpha$ radiation on a Philips PW-1710 diffractometer. Typical 2Θ angular scans ranged between 20° and 80°, in steps varying from 0.02° to 0.05°. The measurements were performed at room temperature and MgO was used as an internal standard. The $Ln NiO_3$ samples were found to have an orthorhombic distorted perovskite structure, belonging to *Pbnm* space group symmetry. Lattice parameters were calculated from the corrected peak positions using a least-squares refinement program (14) for all identified reflections between $20^\circ \leq 2\Theta \leq 80^\circ$.

2.4. Differential Scanning Calorimetry

Differential scanning calorimetry (DSC) analyses were performed on a Shimadzu DSC-50 calorimeter operating at temperatures ranging from 100 to 500 K and under nitrogen flux of $\sim$50 ml/s. The samples, in a powdered form and weighing typically 20 mg, were placed in sealed aluminum crucibles and subjected to both heating and cooling rates of $\sim$10 K/min. An empty aluminum crucible was used as reference in all performed measurements.

2.5. Scanning Electron Microscopy

A Leica–Cambridge S 440 scanning electron microscope was used to observe the microstructure of the samples. These observations were performed using an acceleration voltage of 20 kV and working distance of 10 mm. The samples were attached on a sample holder and recovered with a gold film (25 Å thickness).

2.6. Electrical Resistivity

Electrical resistivity measurements were performed using the so-called four-probe technique. Four copper electrical leads were attached to gold film contact pads with Ag epoxy on $2 \times 3 \times 8$ mm^3 parallelepiped-shaped samples that were dried at 150°C for $\sim$2 min. Electrical resistance as a function of temperature was measured in a cryostat with two current sources, operating at several fixed values of the excitation current, a Keithley 182 nanovoltmeter, and a Keithley 196 multimeter. The samples and a calibrated Pt thermometer are mounted on a parallelepiped-shape copper block to assure the thermal contact. The procedure during measurement was always to cool the sample down to 77 K, apply the excitation current, warm the sample above room temperature, and then cool the sample to 77 K.

3. RESULTS AND DISCUSSION

3.1. X-Ray Diffraction

3.1.1. Kinetics of the phase formation and crystal structure. It is useful to begin this discussion by showing the thermal evolution of the precursors by means of the crystallographic changes they undergo up to the formation of the desired phase. Usually, the precursors preserve their nature at sintering temperatures as high as 300°C. With increasing sintering temperature, the kinetics of the phase formation was accompanied by a detailed analysis of the X-ray powder diffraction data taken on samples heat-treated at different stages during the sintering. Generally speaking, we have performed X-ray diffraction measurements in samples since early stages of crystallization until the desired phase is retained. It is important to notice that most of the data were taken in materials far away from the thermodynamic equilibrium. This implies that changes on both time and temperature of sintering or even in the oxygen pressure used during the heat treatments would affect the results shown below. In any event, since we have produced several samples through different routes, studies like the one described here can also be used to compare methods and the thermal evolution of these compounds.

A typical example of the phase formation obtained through X-ray diffraction patterns of a polycrystalline sample of $NdNiO_3$ compound prepared via sol–gel precursor and sintered at different temperatures and pressures is shown in Fig. 1. The results of a sample heat-treated at 650°C under oxygen pressure of $\sim$30 bar for 48 h (Fig. 1a) reveal the beginning of the $NdNiO_3$ phase formation. The X-ray diffraction pattern shows Bragg reflections belonging to the desired phase but an accurate view of these peaks reveal that they are rather broad. Such a broadening is consistent with small grain sizes, a result of the low-temperature synthesis used to prepare the material. In fact, one would expect that other factors as small differences in stoichiometry across the sample and crystalline defects also contribute to the broadening of the Bragg reflections. On the other hand, the X-ray diagram also reveals vestiges of the most intense reflections belonging to the simple oxide NiO, as marked in the figure. Such an identification is compelling evidence that the material at this early stage of sintering is composed of at least two crystallographic phases: $NdNiO_3$ and NiO. The presence of these two phases also suggests that there must be some Nd_2O_3 remaining in the sample. There are two possibilities for the absence of the Bragg peaks belonging to Nd_2O_3: (1) the simple oxide

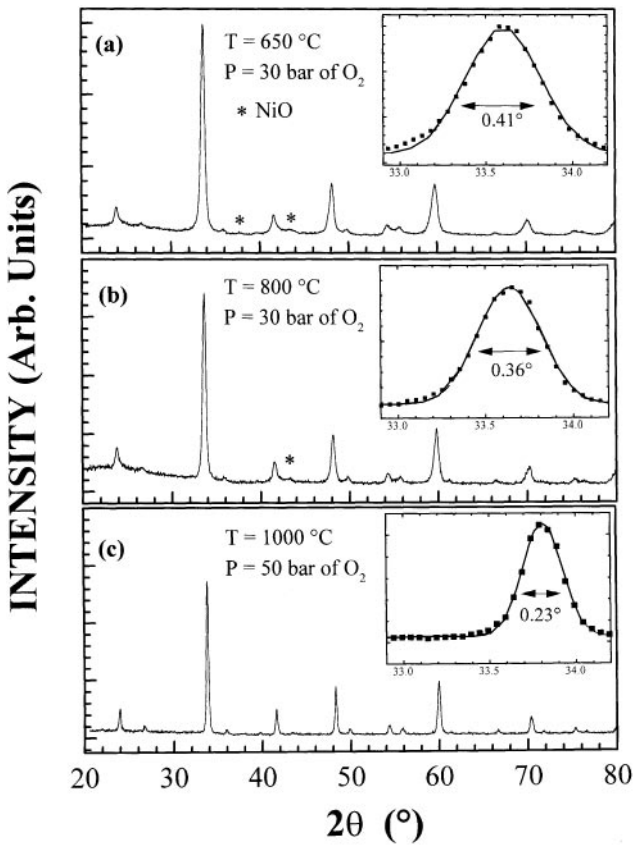

FIG. 1. X-ray diffraction patterns of polycrystalline samples of $NdNiO_3$ prepared through sol–gel precursor and subjected to different heat treatments: (a) 650°C under oxygen pressure of 30 bar; (b) 800°C under oxygen pressure of 30 bar; and (c) 1000°C under oxygen pressure of 50 bar. The insets show an expanded view of the (200)/(020)/(112) reflections to higher 2Θ values and the decrease of the full width at half maximum (FWHM) as discussed in the text.

Nd_2O_3 is presumably in the form of very small particles randomly distributed throughout the sample, by virtue of the preparation technique, which are not detected by X-ray diffraction analysis; and (2) a phase $NdNi_{(1-x)}O_3$ is formed. We argue that the first possibility is likely for two reasons: one, the phase $NdNi_{(1-x)}O_3$ is not known to exist (1–11), and two, because of the detection of peaks belonging to Nd_2O_3 by X-ray diffraction in samples prepared through MO and HY, as discussed below.

An additional heat treatment, performed at 800°C under oxygen pressure of $\sim$30 bar for 48 h, revealed important changes in the X-ray pattern of the material, as shown in Fig. 1b. The most remarkable change observed here is the perceptible narrowing of all reflections belonging to the $NdNiO_3$ phase. A detailed analysis of all Bragg reflections also revealed traces of NiO, or more appropriately, that the material is still composed of two phases. Increasing both the sintering temperature and the oxygen pressure to 1000°C and 50 bar for 48 h, respectively, resulted in single-phase material, as shown in Fig. 1c. This figure displays all the reflections belonging to the $NdNiO_3$ phase and these peaks are much sharper than those displayed in Figs. 1a and 1b. The (*hkl*) indexes (not shown) were assigned on the basis of the $GdFeO_3$-type orthorhombically distorted perovskite structure, *Pbnm* space group symmetry.

It is important to notice that, in the early stage of the sintering process, the mixture is believed to be an intimate mixture of small grains of simple oxides (as NiO and Nd_2O_3) and the desired phase. The mixture is not in thermodynamic equilibrium and the reaction is still incomplete for heat treatments performed at low temperatures and time intervals as short as 48 h. In fact, it seems that the components of the mixture would react with each other after much longer times. The other important variable here is the oxygen pressure to which the powders are subjected during the sintering. From the results described above, it seems the higher the pressure the higher is the degree of crystallization of the compound. On the other hand, the presence of broad peaks certainly can be associated with both the average small grain size and the short-range crystallographic order within physical grains of these powders. In order to put this point in perspective, the broadening of the reflection (200)/(020)/(112) at $\sim$33.7° was analyzed and is shown in the insets of Fig. 1. It is observed that the full width at half maximum FWHM decreases monotonically from 0.41 ± 0.02°, in the sample heat-treated at 650°C under 30 bar of O_2, to 0.23 ± 0.02°, estimated in the sample heat-treated at 1000°C under 50 bar of O_2. This suggests that the Bragg reflections are broadened because of the presence of a large distribution of the lattice parameters in the powder, or more appropriately, to the small differences in stoichiometry across the sample. These results also reveal a clear displacement of the reflection (200)/(020)/(112) to higher 2Θ values. Such a displacement indicates that increasing both sintering temperature and pressure results in a shrinkage of the unit cell volume. We argue that such a behavior is consistent with a higher content within the perovskite phase of Ni^{3+} at expense of larger Ni^{2+} ions.

Similar results to the kinetics of the phase formation described above in samples prepared through sol–gel precursors were found in $NdNiO_3$ compounds prepared through MO and HY precursors. However, the X-ray diffraction diagrams of those MO and HY samples (not shown) revealed Bragg reflections belonging to simple oxides NiO and Nd_2O_3 even in samples sintered at 1000°C under $\sim$50 bar of O_2 for 48 h.

The kinetics of phase formation of other compounds of $LnNiO_3$ (Ln = Pr, Sm) prepared through different methods were slightly different than those observed in $NdNiO_3$ compounds. As far as this point is concerned, it is important to stress some important features found in sintered samples of both Pr and Sm, as shown in the diffractograms of Fig. 2.

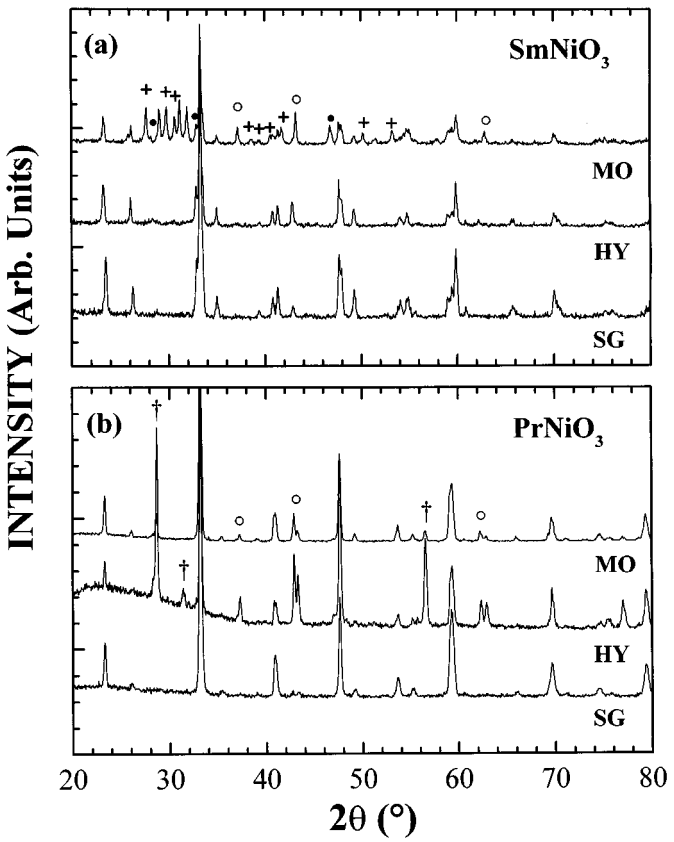

FIG. 2. X-ray diffraction patterns of (upper panel) $SmNiO_3$ and (lower panel) $PrNiO_3$ compounds prepared via different processes: mixture of simple oxides, MO; precipitation of hydroxides, HY; and sol–gel precursors, SG. The symbols represent reflections belonging to different phases observed in these diffractograms: (●) Sm_2O_3; (+) $Sm_2O(CO_3)_2.xH_2O$; (○) NiO; and (†) Pr_6O11.

This figure displays the results of X-ray powder diffraction taken on samples sintered at 1000°C under oxygen pressure of ~70 bar for 72 h. The major difference between the results shown in this figure and those shown in Fig. 1 is related to the achievement of single-phase materials. In fact, single-phase $PrNiO_3$ and $SmNiO_3$ were obtained only when samples were prepared through sol–gel precursors SG and were subjected to heat-treatments at both 1000°C and oxygen pressure of 70 bar for 48 h. The X-ray patterns of these Pr and Sm materials revealed not only the presence of the reflections belonging to the desired phase but also those belonging to simple oxides such as NiO, Sm_2O_3, and Pr_6O_{11}, as shown in Fig. 2. Such a feature suggests that not only prolonged heat treatments under high oxygen pressures are necessary for the progressive elimination of extra phases in these materials. It seems that the nature of the precursor is also an important variable in order to obtain single-phase $LnNiO_3$ (Ln = Pr, Nd, Sm) compounds.

The preceding discussion was confirmed by the X-ray pattern of the $SmNiO_3$ compound, prepared via MO, in which we have identified some intense Bragg reflections belonging to samarium oxide carbonate hydrate, $Sm_2O(CO_3)_2.xH_2O$ (see Fig. 2a). The identification of such an additional phase in samples heat-treated at both high temperatures and oxygen pressures is certainly related to the incomplete reaction between Sm_2O_3 and NiO. In fact, one would expect that an undesirable additional amount of Sm_2O_3 in the mixture reacts with both CO_2 and H_2O of the atmosphere during the cooling process, promoting the formation of this kind of carbonate. Similar oxicarbonate of Ln = La have been observed in samples of La_2CuO_4 prepared via coprecipitation of oxalates (15).

Similar to the results obtained in $SmNiO_3$ samples, single-phase $PrNiO_3$ compounds were found only when the material was prepared via SG route and subjected to heat-treatments at both high temperatures and oxygen pressures. The other samples, prepared via both MO and HY and sintered in the same conditions, resulted in an intimate mixture of $PrNiO_3$ and single oxides as NiO and Pr_6O_{11} (see Fig. 2b). It is important to notice that the presence of additional Bragg peaks during the kinetics of the phase formation, and presumably associated with Pr_6O_{11} and NiO, is hardly noticeable here mostly due to the overlap with reflections belonging to the $PrNiO_3$ phase. However, when these samples were subjected to heat treatments at higher temperatures, the occurrence of the $PrNiO_3$ phase was confirmed by the appearance of reflections occurring at low Bragg angles ($2\Theta \sim 28.5^\circ$), as shown in Fig. 2b. Also, in contrast to diffractograms both $NdNiO_3$ and $SmNiO_3$ samples, X-ray diffractograms of $PrNiO_3$ compounds revealed that samples prepared through MO exhibit much less intense reflections of both NiO and Pr_6O_{11} than samples prepared via HY. We argue that such a feature is related to two main features of the initial powder: (1) the small difference in the stoichiometry across the grains and (2) the different average grain size of these materials. Samples prepared via HY showed smaller grain size than samples prepared through other methods. Thus, these nonstoichiometric small grains when submitted to both high sintering temperature and oxygen pressure, would preferentially promote the stabilization of Pr^{4+} instead of Pr^{3+}. The presence of both Pr^{4+} and high oxygen pressure result in the formation of Pr_6O_{11}, which is inconvenient to the $PrNiO_3$ phase formation. The combined result is the observation of a great number of Bragg peaks belonging to Pr_6O_{11} in samples prepared via HY method.

The results of the X-ray powder diffraction performed on $LnNiO_3$ compounds (Ln = Pr, Nd, Sm) allowed us to better compare our results with those reported in the literature (1–3). Such a comparison was made through the calculated lattice parameters belonging to the orthorhombic structure, *Pbnm* space group, as displayed in Table 1. The lattice parameters were obtained from a refinement of at least 15 indexed reflections belonging to diffractograms taken on

TABLE 1
Calculated Lattice Parameters of $LnNiO_3$ (Ln = Nd, Sm, Pr) Compounds Heat-Treated at 1000°C under Oxygen Pressure of ~ 70 bar

		a (Å)	b (Å)	c (Å)
$NdNiO_3$	MO	5.397	5.386	7.577
	HY	5.391	5.389	7.622
	SG	5.383	5.381	7.615
	Ref. (3)	5.389	5.382	7.610
$SmNiO_3$	MO	5.366	5.452	7.581
	HY	5.357	5.442	7.576
	SG	5.351	5.433	7.575
	Ref. (1)	5.325	5.427	7.561
$PrNiO_3$	MO	5.419	5.385	7.614
	HY	5.413	5.384	7.629
	SG	5.403	5.396	7.649
	Ref. (3)	5.419	5.380	7.626

Note. The lattice parameters of similar compounds given in Refs. (1) and (3) are also listed for a better comparison of the data.

samples subjected to heat treatments at $T = 1000°C$ and under oxygen pressure of 70 bar for ~72 h. It is worth mentioning that not all samples were single phase after the final heat treatment. However, we have calculated the lattice parameters of the multiphase materials by the refinement of the Bragg peaks belonging only to the desired phase $LnNiO_3$. The computed lattice parameters displayed in Table 1 also include the corresponding parameters obtained on polycrystalline samples of $LnNiO_3$ and listed in Refs. (1) and (3). Generally speaking, a careful observation of the lattice parameters a, b, and c listed in Table 1 indicates that our results are in agreement with those reported in the literature. In fact, the reported lattice parameters of these nickelates are comprised in a large range of values. For example, values of the lattice parameters of $NdNiO_3$ were found to be $a = 5.3891$, $b = 5.3816$, and $c = 7.6101$ Å (4), and $a = 5.3895$, $b = 5.3774$, and $c = 7.6079$ Å (16). Similar differences are also found in other nickelates as $PrNiO_3$ and $SmNiO_3$ (1–11). In any event, the results shown in Table 1 also reveal that lattice parameters belonging to $NdNiO_3$ are closer to those listed in Ref. (3).

From the above results it is possible to preliminarily conclude that single-phase $NdNiO_3$ is more easily obtained than either $SmNiO_3$ or $PrNiO_3$ compounds. Indeed, single-phase $NdNiO_3$ compounds were achieved when all precursors were subjected to heat treatments at lower sintering temperatures (~800°C) and under relatively low oxygen pressures (~50 bar), and at short time intervals of ~48 h. On the other hand, samples of $PrNiO_3$ and $SmNiO_3$ showed to be single phase only when subjected to extreme conditions of sintering involving high temperatures of ~1000°C and oxygen pressure of ~70 bar for 72 h. A comparison among the three methods used for producing these materials indicated that sol–gel precursors, when convenient sintered, resulted in both high-quality and single-phase samples of $LnNiO_3$ (Ln = Pr, Nd, Sm) compounds.

3.2. Scanning Electron Microscopy

The morphology of the sintered samples was studied through scanning electron microscopy SEM observations for compounds of $LnNiO_3$ (Ln = Nd, Sm, Pr). Typical results of these characterizations are exemplified by the observations obtained in samples of $SmNiO_3$, which are shown in Fig. 3. This figure shows photomicrographs of three samples prepared through: (a) mixture of simple oxides MO; (b) precipitation of hydroxides HY; and (c) sol–gel precursors SG. A careful inspection of these morphologies reveals interesting features, which were found in all samples studied as follows. The samples prepared through the MO method were much more porous than those prepared through both precipitation and sol–gel precursors, as is easily seen in the figure. The grains were found to have a spherical shape and average grain size (<3 μm). Also, a comparison of these photos reveals a clear difference of the average grain size which is strongly dependent upon the precursor used for the synthesis. For example, samples prepared through MO are comprised of grains as larger as ~2 μm. Other materials, as those prepared through HY and SG routes, exhibit grains with average grain size <1 μm. Also, samples prepared through SG were found to have the smallest average grain size. Indeed, a continuous enhancement of the average grain size from samples prepared by SG toward that prepared through MO is observed. Similar behavior is also found when both the number of agglomerates and the porosity of the samples are invoked. These features strongly suggest that samples prepared through sol–gel are more suitable for a precise microstructural control than others prepared either by MO or HY routes. The features observed in the microstructures of these materials would affect their transport properties, as discussed below.

3.3. Transport Properties

All the samples described above were characterized by means of temperature dependence of the electrical resistivity $\rho(T)$. Some of these results are shown in Fig. 4, which displays the $\rho(T)$ data, taken during the heating process of $PrNiO_3$ and $SmNiO_3$ compounds prepared through sol–gel method and three curves of $NdNiO_3$ samples prepared via mixture of oxides (MO), precipitation of hydroxides (HY), and sol–gel (SG) methods. The most prominent feature of these curves is the occurrence of a metal–insulator phase transition in a large range of temperature $T_{MI} \sim 135$, 200, and 402 K, as observed in $PrNiO_3$, $NdNiO_3$, and $SmNiO_3$,

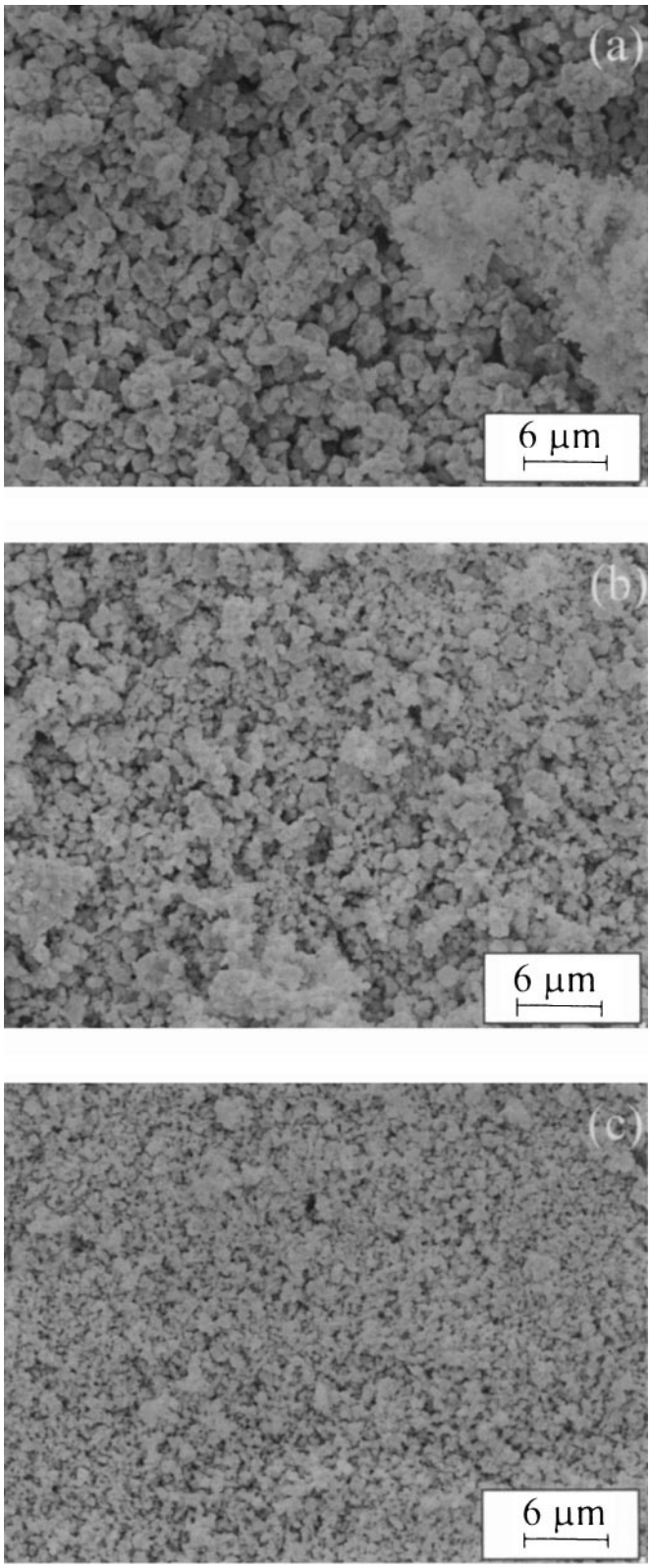

FIG. 3. Observation of the scanning electron microscopy of $SmNiO_3$ samples prepared through three different methods: (a) mixture of simple oxides MO; (b) precipitation of hydroxides HY; and (c) sol–gel precursors SG.

respectively, in complete agreement with other values listed in the literature (2). Such a phase transition was found to be of first-order mostly due to the hysteresis observed in $\rho(T)$ data, as shown in the inset of Fig. 4 for the $NdNiO_3$ sample prepared through sol–gel precursors. This hysteresis is an intrinsic property of these nickelates and differences observed in the $\rho(T)$ data obtained during cooling and heating processes are due to the coexistence of both metallic and insulating phases in a temperature range close to T_{MI} (17). The temperature width which corresponds to the hysteresis was found to be as large as ~ 35 K and compares to typical values of ~ 30 K, as described in Ref. (18).

Returning to the $\rho(T)$ data of Fig. 4. Above T_{MI}, the electrical resistivity increases linearly with increasing temperature. We have found that such a linearbehavior is described as $\rho(T) = \rho_0 + AT$. This behavior is typical for electron–phonon scattering and ρ_0 is the electrical resistivity caused by the scattering of the electrons by static defects within the materials, as nonstoichimetry across the sample. Let us concentrate the discussion on data belonging to samples of $NdNiO_3$ prepared through different precursors. We obtained values of ρ_0 of $\sim 3.3 \times 10^{-5}$, 8.1×10^{-3}, and $6.0 \times 10^{-4}\ \Omega$ cm in samples SG, HY, and MO, respectively. These values of ρ_0 strongly suggest that samples SG are almost free of internal defects and are close to the desired stoichiometry. The values of A were found to be $\sim 8.4 \times 10^{-7}$, 1.6×10^{-5}, and $6.2 \times 10^{-6}\ \Omega$ cm K^{-1}, in samples SG, HY, and MO, respectively. These values are close to those

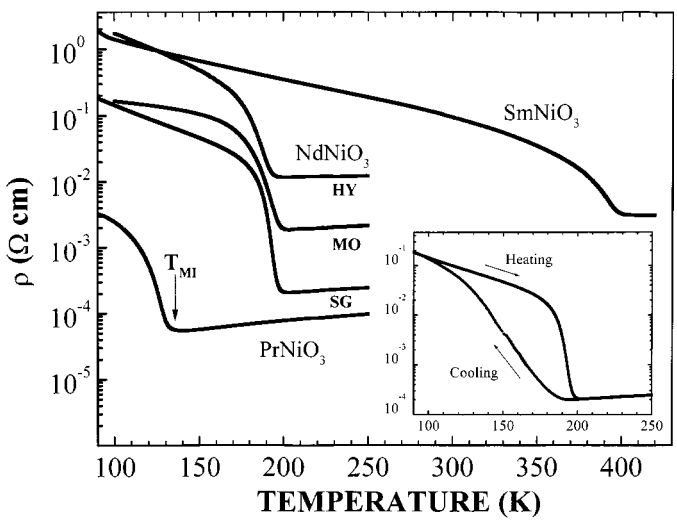

FIG. 4. Temperature dependence of electrical resistivity $\rho(T)$ of polycrystalline samples of $LnNiO_3$ (Ln = Pr, Nd, Sm) prepared through different precursors. The figure shows data taken during the heating process on samples of $LnNiO_3$ (Ln = Pr, Nd, Sm) prepared through sol–gel precursors SG and $NdNiO_3$ samples prepared through precipitation of hydroxides HY and mixture of simple oxides MO. The inset displays the $\rho(T)$ data taken during both the heating and cooling processes in the $NdNiO_3$ sample prepared through sol–gel precursors SG.

found in related nickelates (7, 19). Below T_{MI}, the electrical resistivity of all samples studied exhibits a semiconducting-like behavior. Attempts were made to fit the $\rho(T)$ resistivities in a large range of $T < T_{MI}$ to well-known scattering mechanisms such as correlated and noncorrelated variable-range hopping as well as a simple activation process dependence. It is worth mentioning that all of these fits failed for the temperature range investigated.

A careful inspection of Fig. 4 also shows that the electrical resistivity of these samples jumps by a few orders of magnitude at T_{MI}. The results of $NdNiO_3$ reveal that changes in the magnitude of $\rho(T)$ close to T_{MI} are sample dependent and certainly related with the precursor used to synthesize these compounds. In fact, the metal–insulator transition width is much sharper in the SG sample and $\rho(T)$ increases $\sim 10^2$ times of its magnitude in the temperature range from 200 to 180 K. These changes are much less pronounced in samples prepared through MO and HY methods: they are about 15 and 10 times, respectively, for the same temperature interval. Such an abrupt change in the magnitude of $\rho(T)$ is intrinsic to the materials, i.e., it is microstructure independent and associated with the properties within the grains. These results also indicate that samples prepared through SG method have much more homogeneous grains and that small differences in the stoichiometry within the grains of the sample, as discussed above, determine the changes observed in $\rho(T)$ at temperatures close to T_{MI}. Results similar to those shown in Fig. 4 were observed in both $SmNiO_3$ and $PrNiO_3$ samples. However, it is important to notice that samples of these compounds prepared through either HY and MO processes were not single-phase materials, and contributions to the electrical resistivity of extra phases can be responsible for these differences.

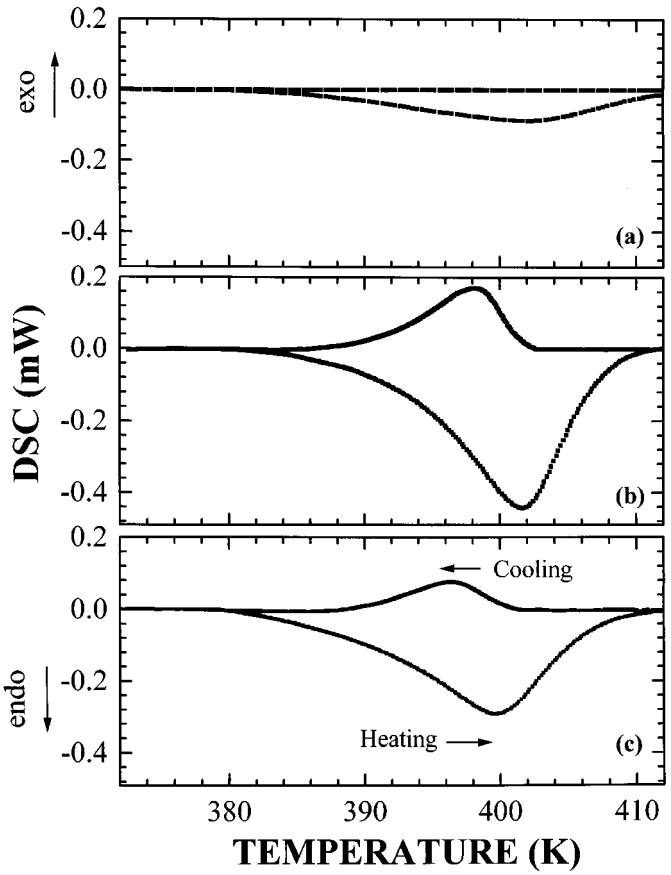

FIG. 5. Temperature dependence of the differential scanning calorimetric measurements of $SmNiO_3$ samples prepared through different methods: (a) mixture of simple oxides; (b) precipitation of Ln^{3+} and Ni^{3+} hydroxides; and (c) sol–gel precursor.

3.4. Differential Scanning Calorimetry

The differential scanning calorimetric (DSC) analysis is an alternative method in determining the metal–insulator transition temperature T_{MI} and to infer about the nature of the phase transition in these compounds. We have performed these measurements on samples of $NdNiO_3$ and $SmNiO_3$ prepared through different precursors in a temperature range from 100 to 600 K. These measurements were performed upon both cooling and heating processes. A common feature observed in these measurements was the occurrence of two peaks at temperatures near T_{MI}, as determined by the electrical resistivity data: (1) one endothermic peak, observed during the heating process; and (2) one exothermic peak on the cooling process. Some of these characterizations are shown in Fig. 5, which displays an expanded view of the DSC measurements performed on $SmNiO_3$ compounds prepared through three different routes. The first point to be addressed here concerns the nature of the transition at T_{MI}. The results shown in Fig. 5, or more appropriately the occurrence of two peaks in these experiments, have enabled us to confirm the first-order phase transition at T_{MI} in our samples. In addition, a careful analysis of the data reveals that the metal–insulator transition temperature, defined as the maximum value of the endothermic peaks, varies slightly from sample to sample and it was found to be between ~ 396 and 402 K. This is a small variation in temperature and we assume that $T_{MI} \sim 400$ K is nearly constant for these series, which is in excellent agreement with the T_{MI} values found in the literature for $SmNiO_3$ compounds (2, 20, 21). It is also worth mentioning that DSC curves of polycrystalline samples of $NdNiO_3$ (not shown) were similar to those shown in Fig. 5, and they exhibited $T_{MI} \sim 200$ K. These T_{MI} values are in excellent agreement with those obtained from $\rho(T)$ data shown in Fig. 5 and with the DSC data found in the literature (2, 21).

Returning to the results of Fig. 5. Measurements performed during the cooling down process show exothermic peaks only in samples prepared by SG and HY methods.

These values of the transition temperature were $T_{MI} \sim 398$ K and $T_{MI} \sim 396$ K for samples of HY and SG, respectively. The absence of an endothermic peak in samples prepared through MO process suggests that these samples have a high degree of defects and that differences in non-stoichiometry across the materials are evident. Another interesting feature of these experiments is related with the difference on area peaks of the DSC measurements. Such an area is directly related to the thermal energy released and absorbed during both the warming up and the cooling down process, respectively. We have found that values obtained for the enthalpy changes are $\Delta H \sim 0.2$ J/g to sample prepared via MO, $\Delta H \sim 1.4$ J/g to sample through HY, and $\Delta H \sim 1.1$ J/g to sample obtained through SG on the heating process. These values were slightly smaller than those found in literature of ~ 2.0 J/g and 2.4 J/g (2, 10), as discussed below.

A comparison of X-ray powder diffraction results and data from Ref. (21) showed that enthalpy changes at T_{MI} were related to the crystallinity of the samples. It was observed that ball-milled samples showed smaller values of enthalpy at T_{MI} and that such an effect was attributed to a gradual increase of amorphization of the material (21). It seems that our $SmNiO_3$ samples prepared through MO process have a high degree of disorder and, consequently, a lower value of ΔH at T_{MI}.

It is important to notice that it was not possible to perform the DSC measurements on the $PrNiO_3$ compounds. This may have occurred due to a high degree of internal defects throughout the samples, as discussed in Ref. (20). On the other hand, the results obtained in $NdNiO_3$ samples were very similar to those described above for $SmNiO_3$ compounds. The temperatures in which the MI transition occurs were found to be $T_{MI} \sim 190$, 194, and 197 K in samples prepared through SG, HY, and MO, respectively. These values of T_{MI} differ in less than 10 K from those found in electrical resistivity measurements and strongly suggest that all samples are mostly comprised of the desired $NdNiO_3$ phase. These results are also in agreement with the X-ray diffraction data which showed single-phase materials in all samples prepared through different methods. As far as the enthalpy variation ΔH close to T_{MI} is concerned, we have found values of $\Delta H \sim 1.13$, 1.24, and 0.07 J/g, in samples prepared through SG, HY, and MO, respectively. These ΔH values are very close to those listed in the literature of 1.1 (2), 1.6 (6), and 1.4 J/g (12).

In view of the above DSC results, we infer that $LnNiO_3$ (Ln = Nd, Sm) exhibits a metal–insulator phase transition at temperatures of $T_{MI} \sim 200$ and 400 K, respectively. Such a phase transition occurs at temperatures close to those obtained through electrical resistivity measurements. The DSC data also revealed two peaks close to T_{MI}: one endothermic, observed during the heating, and an exothermic, during the cooling. These two features confirmed the first-order character of the metal–insulator phase transition at T_{MI}.

4. CONCLUSION

In summary, we have produced polycrystalline samples of $LnNiO_3$ (Ln = Pr, Nd, Sm) through three different routes: (1) mixture of simple oxides MO; (2) through coprecipitation of binary hydroxides HY; and (3) via sol–gel precursors SG. From the results of X-ray powder diffraction XRD, we have found that samples of these nickelates crystallize in the $GdFeO_3$-type orthorhombically distorted perovskite structure, *Pbnm* space group symmetry. The XRD results also revealed that single-phase materials were mostly those samples prepared through sol–gel precursor. Measurements of electrical resistivity $\rho(T)$ revealed that $LnNiO_3$ compounds display a first-order metal–insulator MI transition at temperatures $T_{MI} \sim 135$, 200, and 400 K, for Ln = Pr, Nd, Sm; respectively. Such a first-order nature of the transition was confirmed by the occurrence of hysteresis in the $\rho(T)$ data at temperatures close to T_{MI}. Also, the T_{MI} values were found to be in excellent agreement with those reported in the literature. Differential scanning calorimetric DSC measurements confirmed the first-order character of the transition occurring at T_{MI} and the corresponding transition temperatures obtained via $\rho(T)$ data. A comparative study involving samples prepared through three different processes and characterizations by means of XRD, $\rho(T)$, SEM, and DSC suggests that samples prepared through sol–gel precursors are more homogeneous than those prepared through the mixture of simple oxides and coprecipitation of binary hydroxides.

ACKNOWLEDGMENTS

The authors have benefited from the technical assistance of Walter Soares de Lima. This work was supported by the Brazilian agency Fundação de Amparo à Pesquisa do Estado de São Paulo (FAPESP) under Grants 96/08614-4 and 99/10798-0. One of us (M.T.S.) is a FAPESP fellow under Grant 97/11369-0, and R.F.J. is a Conselho Nacional de Desenvolvimento Científico e Tecnológico (CNPq) fellow under Grant 304647/90-0.

REFERENCES

1. G. Demazeau, A. Marbeuf, M. Pouchard, and P. Hagenmuller, *J. Solid State Chem.* **3,** 582 (1971).
2. M. L. Medarde, *J. Phys. Condens. Matter* **9,** 1679 (1997).
3. P. Lacorre, J. B. Torrance, J. Pannetier, A. I. Nazzal, P. W. Wang, and C. Huang, *J. Solid State Chem.* **91,** 225 (1991).
4. J. L. García-Muñoz, J. Rodríguez-Carvajal, P. Lacorre, and J. B. Torrance, *Phys. Rev. B* **46,** 4414 (1992).
5. J. B. Torrance, P. Lacorre, A. I. Nazzal, E. J. Ansaldo, and Ch. Niedermayer, *Phys. Rev. B* **45,** 8209 (1992).
6. X. Granados, J. Fontcuberta, X. Obradors, and J. B. Torrance, *Phys. Rev B* **46,** 15,683 (1992).

7. X. Granados, J. Fontcuberta, X. Obradors, L. Mañosa, and J. B. Torrance, *Phys. Rev* **48,** 11666 (1993).
8. M. Medarde, P. Lacorre, K. Conder, F. Fauth, and A. Furrer, *Phys. Rev. Lett*. **80,** 2397 (1998).
9. J. A. Alonso, J. L. Garcia-Munoz, M. T. Fernandes-Diaz, M. A. G. Aranda, M. J. Martinez-Lope, and M. T. Casais, *Phys. Rev. Lett*. **82,** 3871 (1999); J. A. Alonso, M. J. Martinez-Lope, M. T. Casais, M. A. G. Aranda, and M. T. Fernandes-Diaz, *J. Am. Chem. Soc*. **121,** 475 (1999).
10. I. Vobornik, L. Perfetti, M. Zacchigna, M. Grioni, G. Margaritondo, J. Mesot, M. Medarde, and P. Lacorre, *Phys. Rev. B* **60,** R8426 (1999).
11. J. K. Vassiliou, M. Hornsbostel, R. Ziebarth, and F. J. Disalvo, *J. Solid State Chem.* **81,** 208 (1989).
12. J. Perez-Cacho, J. Blasco, J. Garcia, and J. Stankiewicz, *Phys. Rev. B* **59,** 14,424 (1999).
13. See, for instance, R. F. Jardim, L. Ben-Dor, and M. B. Maple, *J. Alloys Compounds* **199,** 105 (1993); P. A. Suzuki and R. F. Jardim, *Physica C* **267,** 153 (1996).
14. M. Calligaris and S. Geremia, "X-Ray Powder Programmers on IBM Compatible PC." ICTP, Italy, 1989.
15. A. J. P. Andrade, A. J. S. Machado, and R. F. Jardim, *Mater. Lett*. **13,** 96 (1992).
16. J. L. Garcia-Muñoz, M. Suaaidi, M. J. Martínez-Lope, and J. A. Alonso, *Phys. Rev. B* **52,** 13,563 (1995).
17. X. Granados, J. Fontcuberta, X. Obradors, L. Manosa, and J. B. Torrance, *Phys. Rev. B* **48,** 11,666 (1993).
18. X. Granados, J. Fontcuberta, X. Obradors, and J. B. Torrance, *Phys. Rev. B* **46,** 15,683 (1993).
19. K. P. Rajeev, G. V. Shivashankar, and A. K. Raychaudhuri, *Solid State Commun.* **7,** 591 (1991).
20. J. Pérez-Cacho, J. Blasco, J. Garcia, M. Castro, and J. Stankiewicz, *J. Phys.: Condens. Matter* **11,** 405 (1999).
21. G. Frand, O. Bohnke, P. Lacorre, J. L. Fourquet, A. Carré, B. Eid, J. G. Théobald, and A. Gire, *J. Solid State Chem.* **120,** 157 (1995).